Available online at www.sciencedirect.com
ScienceDirect
Sensors and Actuators A 142 (2008) 561–568
SENSORS AND ACTUATORS A PHYSICAL
www.elsevier.com/locate/sna

A 3D micromechanical compass

Jukka Kyynäräinen [a,*], Jaakko Saarilahti [a], Hannu Kattelus [a], Anu Kärkkäinen [a], Tor Meinander [a], Aarne Oja [a], Panu Pekko [a], Heikki Seppä [a], Mika Suhonen [a], Heikki Kuisma [b], Sami Ruotsalainen [c], Markku Tilli [d]

[a] *VTT Technical Research Centre of Finland, P.O. Box 1000, FI-02044 VTT, Finland*
[b] *VTI Technologies Oy, P.O. Box 27, FI-01621 Vantaa, Finland*
[c] *Suunto Oy, Valimotie 7, FI-01510 Vantaa, Finland*
[d] *Okmetic Oyj, P.O. Box 44, FI-01301 Vantaa, Finland*

Received 12 January 2007; received in revised form 20 August 2007; accepted 21 August 2007
Available online 2 September 2007

Abstract

We have designed and fabricated micromechanical magnetometers intended for a 3D electronic compass which could be embedded in portable devices. The sensors are based on the Lorentz force acting on a current-carrying coil, processed on a single crystal silicon resonator, and they are operated in vacuum to reach high enough Q values. Sensors for all cartesian components of the magnetic field vector can be processed on the same chip. The vibration amplitude is detected capacitively and the resonance is tracked by a phase-locked-loop circuit. The fabrication process is based on aligned direct bonding of a double side polished silicon wafer and a SOI wafer. Magnetometers measuring the field component along the chip surface have a flux density resolution of about 10 nT/$\sqrt{\text{Hz}}$ at a coil current of 100 μA. Magnetometers measuring the field component perpendicular to the chip surface are currently less sensitive with a flux density resolution of about 70 nT/$\sqrt{\text{Hz}}$. The standard deviation of the signal was less than 1% over a period of a few days.

Keywords: Magnetometers; Micromechanics; MEMS; Resonant sensors

1. Introduction

The demand for navigation aids in portable instruments like watches, mobile phones, etc., is growing. Often orientation information is sufficient instead of position information, and a simple magnetic compass is a cost-effective solution in this case. An electronic magnetic compass is also useful to assist satellite navigators in shadow areas. Several types of miniatyrized magnetometers are commercially available but their performance is still limited. For example, magnetoresistive sensors feature high sensitivity but suffer from large offset and drift. Hall sensors have low sensitivity and large offset and temperature dependence. Although 3D magnetometers in a single package are available, the sensing elements are almost always on two or more sensor chips, increasing size and manufacturing costs.

Micromachined magnetometers have been developed before by several authors. They can be classified into two categories by the operating principle, either the torque exerted by the magnetic field on a magnetized material [1] or the Lorentz force acting on a current-carrying conductor [2–4]. The first approach can lead to lower power consumption but we opted for Lorentz force based sensors owing to their potentially simpler fabrication and better stability.

The Lorentz force F acting on a straight conductor or the torque τ acting on a torsionally suspended current loop in an external magnetic field B is given by:

$$\vec{F} = i_c \vec{L} \times \vec{B} \tag{1a}$$

$$\vec{\tau} = i_c \vec{S} \times \vec{B} \tag{1b}$$

where i_c is the coil current, L the length of the conductor, and S is the area of the current loop. Fundamental resolution or minimum detectable magnetic field within a given bandwidth W is limited

* Corresponding author. Tel.: +358 20 7224343; fax: +358 20 7227012.
E-mail address: jukka.kyynarainen@vtt.fi (J. Kyynäräinen).

0924-4247/$ – see front matter © 2007 Elsevier B.V. All rights reserved.
doi:10.1016/j.sna.2007.08.025

by the thermomechanical force or torque:

$$f_{n,m} = \sqrt{4k_B T R_m W} \quad (2a)$$

$$\tau_{n,m} = \sqrt{4k_B T R_I W} \quad (2b)$$

where T is temperature and k_B is the Boltzmann constant. The resonator Q-value is related to the damping factors R_m and R_I by:

$$Q = \frac{2\pi f_m m}{R_m} \text{ or} \quad (3a)$$

$$Q = \frac{2\pi f_m I}{R_I} \quad (3b)$$

where f_m, m and I and are the resonator's mechanical resonance frequency, mass and moment of inertia, respectively. Fundamental resolution is then given by:

$$B_{min} = \frac{f_{n,m}}{F} B \text{ or} \quad (4a)$$

$$B_{min} = \frac{\tau_{n,m}}{\tau} B. \quad (4b)$$

Angular resolution φ_{min} depends on the angle φ between the magnetic field direction and the magnetometer's active axis as:

$$\varphi_{min} = \frac{f_{n,m}}{F_{max} \cos\varphi} \text{ or} \quad (5a)$$

$$\varphi_{min} = \frac{\tau_{n,m}}{\tau_{max} \cos\varphi} \quad (5b)$$

where F_{max} and τ_{max} are the Lorentz force and torque at $\varphi = 90°$. We have calculated angular resolutions at $\varphi = 45°$, since two orthogonal sensors are employed for each direction angle. Angular resolution depends on the magnitude of the flux density as well. We have assumed $B = 10\,\mu T$, corresponding to the horizontal component of the Earth's field in northernmost Europe.

Our goals were to integrate micromechanical magnetometers for all three coordinate axes on one silicon chip and to optimize the sensor resolution to power consumption ratio. These results have been presented earlier in shorter form [5].

2. Magnetometer design

The principle of the magnetometers is shown in Figs. 1 and 2. The sensors are operated in vacuum at their mechanical resonance frequency for better sensitivity. Torsional resonators and a double-ended tuning fork type (detf) resonator detect the magnetic field component along and perpendicular to the chip surface, respectively. In both cases, multi-turn excitation coils were processed on the sensors to enhance the sensitivity. The vibration amplitude is detected capacitively by the sense electrodes. The arrangement of the sense electrodes in both magnetometer types allows the use of a differential readout.

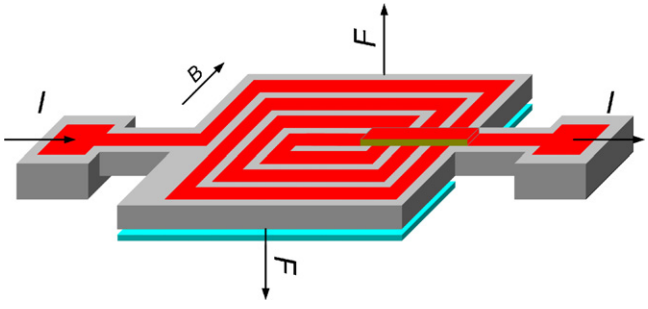

Fig. 1. Principle of the torsional magnetometer. The sense electrodes are located under the moving plate.

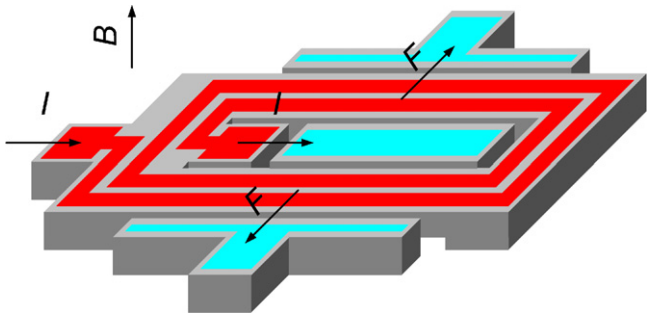

Fig. 2. Principle of the dual-ended tuning fork magnetometer. The two tines share the central sense electrode and have additional sense electrodes on each side of the sensor.

Sensor dimensions were chosen to reach an angular resolution of about 0.2° at 10 Hz measurement bandwidth while not exceeding $i_c = 100\,\mu A$, assuming that high enough Q values can be reached. All sensors were fabricated on SOI wafers with a 20 μm device layer thickness. The lateral dimensions of the torsional resonators varied between 0.5 mm × 0.5 mm and 1.4 mm × 1.4 mm and the length of the detf sensor tines (beams) was 2 mm. The number of excitation coil turns varied between 65 and 125 in the torsional sensors and was either 5 or 10 in the detf sensors. The resonance frequency varied between 8 and 24 kHz for the torsional sensors and was about 50 kHz for the detf sensors. The air gap under the torsional sensor plate was 1 μm at first but was later increased to 1.5 and 2 μm to improve the Q values. The sense capacitances varied between $C_0 = 0.4$ and 1.2 pF for the torsional sensors whereas the geometry of the detf sensor limits their sense capacitances to about 0.1 pF due to overetching of the vertical air gaps.

The excitation coil geometry was chosen to maximize both the signal to thermomechanical noise ratio and the ratio of the Lorentz force to the power dissipated by the coil. To fulfil both requirements, the number of coil turns was maximized but keeping the coil resistance below 30 kΩ in order to reach large enough coil current from a 3 V source.

3. Readout electronics

Capacitive readout was chosen owing to its low noise and power consumption. To keep the electronics as simple as possible, the sense electrodes were charge biased from a battery through $R_b = 10\,M\Omega$ resistors (Fig. 3). The effective signal voltage is then given by:

$$e = \frac{V_b C'}{C_0} \sin\omega t \quad (6)$$

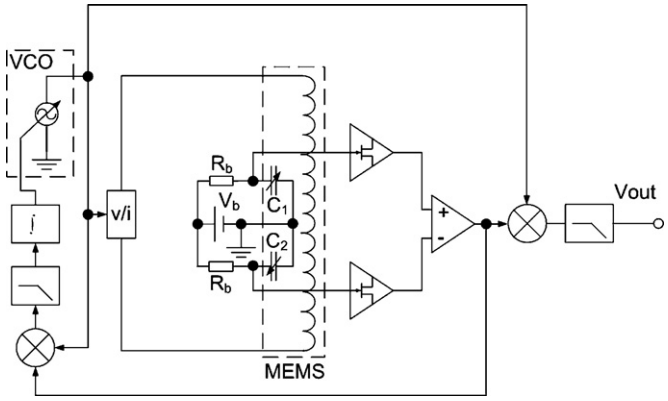

Fig. 3. Schematic diagram of the measurement set-up. VCO is a voltage controlled oscillator and v/i is a voltage to current converter.

where V_b is the dc bias voltage and C' is the changing capacitance for detf and torsional magnetometers, respectively

$$C' = C_0 \frac{x}{d} \tag{7a}$$

$$C' = C_0 \frac{c \tan \varphi}{d - c \tan \varphi}. \tag{7b}$$

Here x is the deflection amplitude of the detf sensor tines, φ the angular deflection amplitude of the torsional sensor, and d is the air gap defining the sense capacitors. Excitation was generated by a voltage-controlled oscillator driving a voltage-to-current converter, shown in Fig. 4. The circuit keeps the centre point of the excitation coil close to ground potential to compensate crosstalk and electrostatic excitation. These are consequences of the rather large capacitance between the coil and the underlying silicon structure which, although grounded, has some residual ac potential due to the resistivity of silicon. The effect of crosstalk could be reduced by measuring the vibration amplitude using a balanced ac bridge configuration with a frequency well above the resonance frequency. This would, however, increase power consumption.

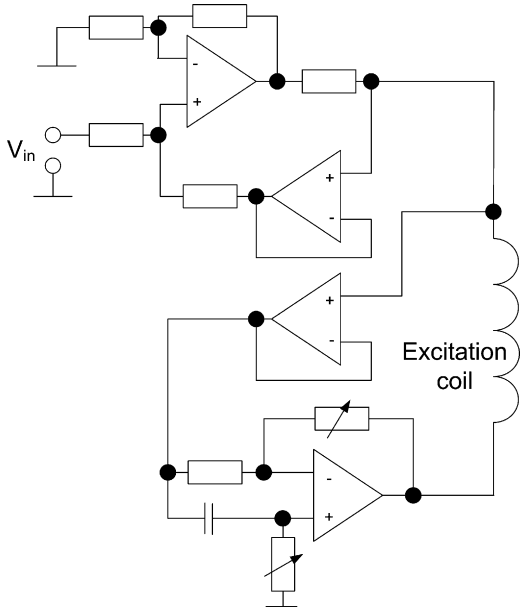

Fig. 4. The voltage-to-current converter circuit to drive the excitation coil.

A phase-locked loop was employed for resonance tracking. The amplitude signal is detected using phase-sensitive readout techniques. An electrostatic force feedback was also tested with the torsional sensors to shorten the settling time which would otherwise be long, on the order of Q_m/f_m, for high-Q resonators. All the measurements presented here were carried out without feedback.

The power consumption of the readout circuit was not studied in this work, as the setup was assembled either from laboratory measurement instruments or discrete components.

4. Noise analysis

The noise model is shown in Fig. 5. Here $v_{n,a}$ is the FET voltage noise density

$$v_{n,a}^2 = \frac{8}{3} \frac{k_B T}{g_m} \tag{8}$$

where g_m is the transconductance of the FET. The thermal noise current density of the FET is given by:

$$i_{n,a}^2 = \frac{k_B T \omega^2 C_{gs}^2}{g_m} \tag{9}$$

and the shot noise current density by:

$$i_{n,g}^2 = 2eI_g \tag{10}$$

where C_{gs} is the gate-to-source capacitance of the FET, e the electron charge and I_g the gate leakage current of the FET. The total noise current density is:

$$i_{n,tot}^2 = i_{n,a}^2 + i_{n,g}^2 \tag{11}$$

which can be converted to noise voltage density as follows:

$$\begin{aligned} v_{n,i}^2 &= i_{n,tot}^2 |R_b||(C_0 + C_a)|^2 \\ &= i_{n,tot}^2 \frac{R_b^2}{1 + \omega^2 R_b^2 (C_0 + C_a)^2} \end{aligned} \tag{12}$$

The Johnson noise voltage density of the bias resistor $v_{n,Rb} = \sqrt{4k_B T R_b}$ is seen at the preamplifier input as:

$$\tilde{v}_{n,R_b} = \frac{\sqrt{4k_B T R_b}}{\sqrt{1 + \omega^2 R_b^2 (C_0 + C_a)^2}} \tag{13}$$

where C_a is the preamplifier input capacitance. The Johnson noise due to resistivity of silicon is negligible compared to other noise sources.

Finally, the voltage noise density $v_{n,m}$ caused by the thermomechanical noise force density, seen at the preamplifier input, is

$$v_{n,m} = \frac{V_b C_n'}{C_0} \frac{\omega^2 R_b^2 C_0 (C_0 + C_a)}{1 + \omega^2 R_b^2 (C_0 + C_a)^2} \tag{14}$$

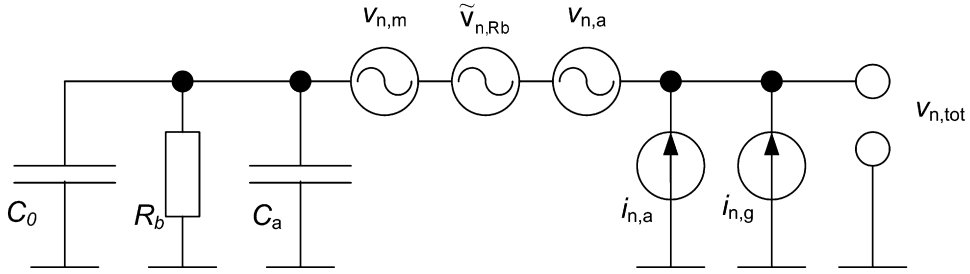

Fig. 5. Noise model for the readout electronics.

where the capacitance change C'_n can be obtained by replacing the deflection amplitudes in Eqs. (7a) and (7b) by their appropriate noise-induced values.

The total noise voltage density is then given by:

$$v^2_{n,tot} = v^2_{n,m} + v^2_{n,a} + v^2_{n,i} + \tilde{v}^2_{n,Rb} \quad (15)$$

Analysis shows that the thermomechanical noise dominates at $Q > 100$ for the detf sensor and about $Q > 1000$ for the torsional sensor. Below these Q values the Johnson noise of the bias resistor is the dominating noise source. In the calculation we assumed the following parameter values, typical for a JFET BF545B: $C_{gs} = 3$ pF, $g_m = 3$ mS, and $I_g = 0.5$ pA. The capacitance C_a was assumed to be 6 pF.

Magnetometer readout could alternatively be implemented by vibrating the sensor electrostatically and by sensing the voltage induced in the coil [6]. One can easily see that in this case the signal-to-noise level is optimized by a single-turn coil with maximum conductor width. With all practical parameter values the noise level would be, however, dominated by the Johnson noise voltage density of the coil resistance instead of the thermomechanical noise. This leads to worse magnetic field resolution, as compared to the capacitive readout technique.

5. Sensor fabrication

The fabrication process was based on aligned direct bonding of a double side polished (DSP) and a SOI wafer. The process included 14 lithography steps, 10 stepper masks, 4 contact masks, and one contact mask for alignment marks. Internal stresses in thin films, induced by differential thermal expansion and deposition, were compensated by metallizing also the backside of the moving silicon plate and by fine tuning the thin film mechanical stresses. Three batches of sensors were fabricated and functional devices were obtained in every batch.

The process started by ICP deep etching of 1 μm deep cavities on the 20 μm thick structure layer of the p-type, 20 μm/1 μm/380 μm thick, 100 mm SOI wafers, followed by growth and patterning of 400 nm thick thermal oxide and the metallic electrodes (Fig. 6a). The wafer bonding surfaces were protected against aluminium impurities by applying lift-off resist twice. Growth of aluminium hillocks was prevented by applying a 350 nm/50 nm thick Mo/Al double-layer metallization on the electrode surfaces. The mechanical stress of the deposited Mo layer was adjusted during the deposition process into a low value of −50 MPa. The control of the thin film thicknesses

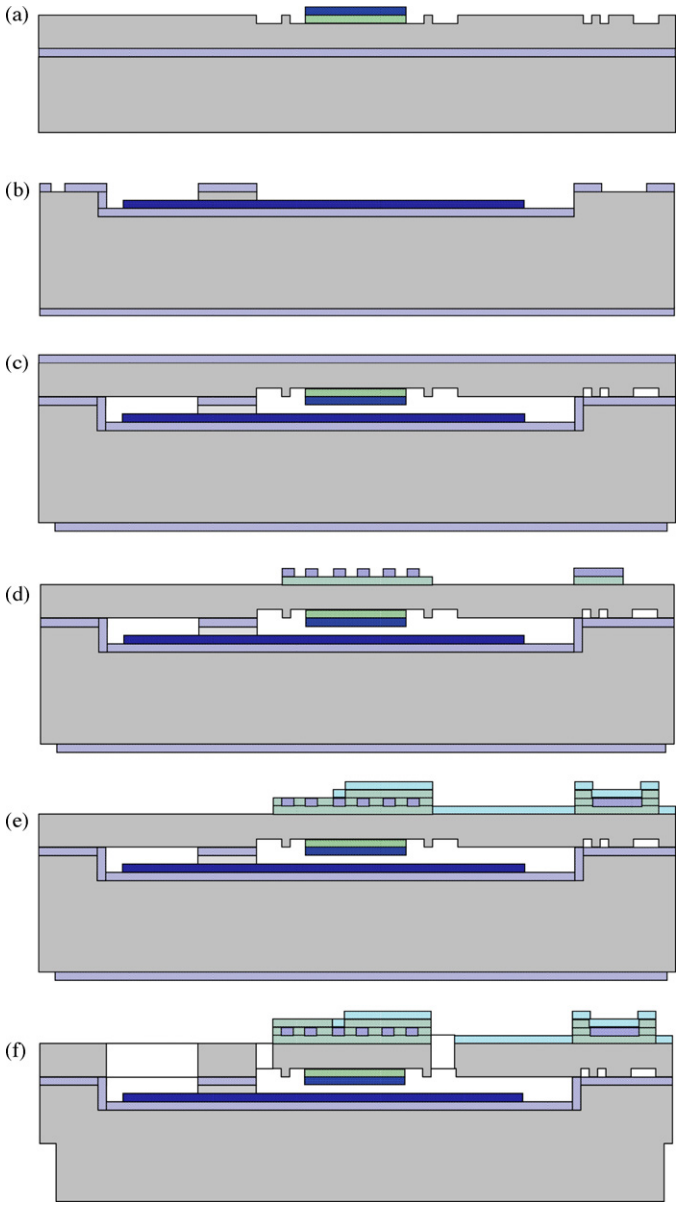

Fig. 6. The main steps of the manufacturing process. (a) Patterning of the antistiction studs and metallizing of the coil metal compensation layers. (b) Cavity etching and metallizing of the sense electrodes for torsional sensors. (c) Direct wafer bonding, followed by removal of the SOI wafer handle layer. (d) Patterning of the excitation coil. (e) Deposition of the isolation and the bridge metal layers. (f) Release etch.

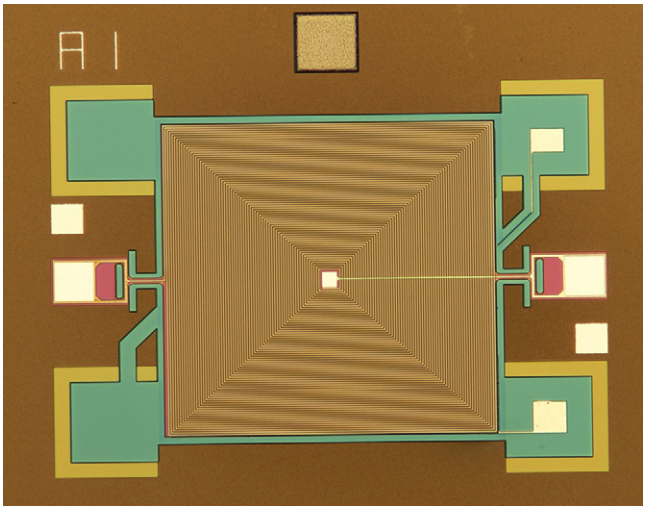

Fig. 7. Photograph of a torsional sensor with a moving plate size of 1 mm × 1 mm.

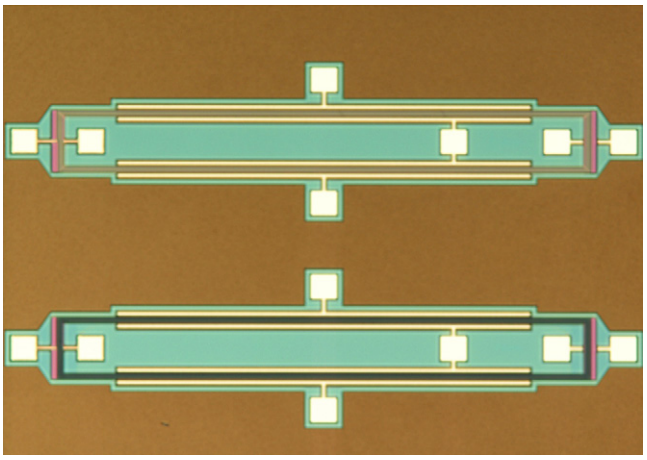

Fig. 8. Photograph of dual-ended tuning fork magnetometers.

as well as the internal mechanical stresses were critical, since the aspect ratio between the capacitor cavity and the lateral dimensions of the moving silicon plate was about 1:1000. The cavity and the electrode metallization of the p-type, 380 μm thick DSP wafers were processed in a similar way (Fig. 6b). The capacitor structure was constructed by low-temperature (200 °C) aligned direct bonding of DSP and SOI wafers, followed by removal of the 380 μm thick handle layer by ICP etching (Fig. 6c). Due to the narrow gap between the electrodes, processing temperatures were restricted below 250 °C during the remaining process steps. The 1 μm thick thermal oxide layer of the SOI wafer was used as the lower insulator layer between the excitation coil and the ⟨Si⟩. Patterning of the thermal oxide as well as growth and patterning of the 500 nm thick excitation Mo coil were aligned on the backside alignment marks in order to obtain the total alignment accuracy of 1 μm through the whole sensor (Fig. 6d). A 50 nm thick ALD aluminium oxide layer, grown at 250 °C processing temperature, was chosen as the insulating layer between the Mo excitation coil and the Al bridge metallization (Fig. 6e). Finally, the moving parts of the device were released by direct ICP deep etching (Fig. 6f). Photographs of the sensors are shown in Figs. 7 and 8.

6. Measurement results

6.1. Q-values

Resonator Q-values were measured as a function of pressure and are shown in Fig. 9. The Q values of the torsional sensors were limited by gas damping even at the lowest pressure attainable by a mechanical vacuum pump (about 6 μbar). The highest Q values, over 30,000, were measured with the smallest-area torsional resonators with a plate size of 0.5 mm × 0.5 mm. Resonators with a plate size of 1 mm × 1 mm and 1.4 mm × 1.4 mm reached Q-values of about 8000 and 4000, respectively. The Q values could be improved by perforating the torsional plate at the expense of the area available for the excitation coil and sense electrodes.

In the detf sensors, the Q values saturated at about 10,000 at pressures below 0.01 mbar. The Q value may be limited by losses in the deforming metallic coil or energy leak through the anchoring points.

The response to an external magnetic field was measured by employing a three-axis Helmholtz coil system outside a nonmagnetic vacuum chamber. The field strength was calibrated using a fluxgate sensor. Magnetometers chips were glued and wire bonded to alumina substrates which, in turn, were mounted on preamplifier boards. Care was taken that all cables and connectors close to the magnetometers were nonmagnetic.

To determine the magnetic field resolution, the height of the thermomechanical noise induced resonance peak was measured using a spectrum analyzer at zero coil current. This was compared to the signal voltage of the phase-sensitive detector at various external magnetic fields. As a consistency check, resolution was also calculated from the measured Q values. Examples are shown in Figs. 10 and 11. In the case of the torsional sensors the agreement was good whereas in the case of the detf

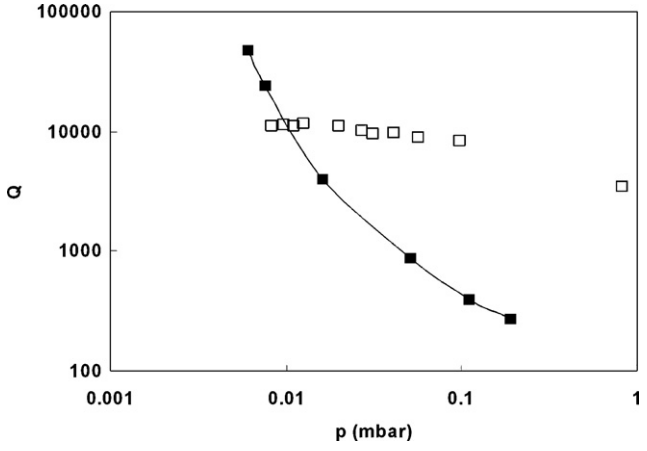

Fig. 9. Measured Q-values of a 0.5 mm × 0.5 mm sized torsional sensor (solid symbols) and a detf sensor (open symbols) as a function of pressure. The line is drawn to guide the eye.

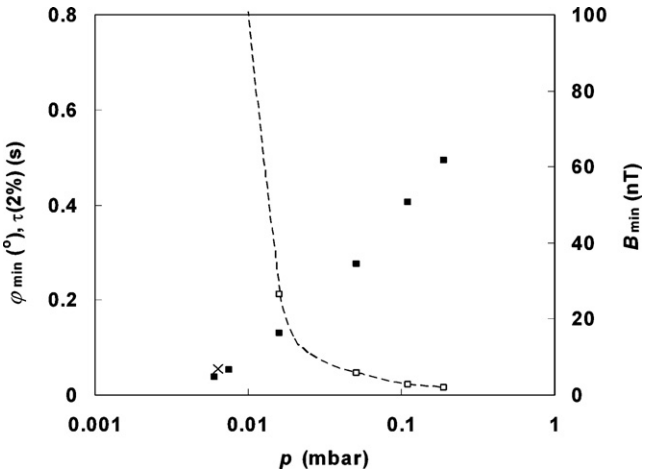

Fig. 10. Angular resolution φ_{min} and minimum detectable magnetic flux density B_{min} of a 0.5 mm × 0.5 mm sized torsional sensor, calculated from the measured Q-values, are marked by the filled squares. Measured flux density resolution of the torsional sensor is shown by the cross and the calculated settling time τ (2%) by the open squares. The line is drawn to guide the eye.

sensors the measured resolution was about 20% worse than the resolution deduced from the Q values. This may be due to unaccounted parasitic capacitances or preamplifier noise, etc. All the torsional sensors of different sizes reached a flux density resolution of about 10 nT/$\sqrt{}$Hz at a coil current of 100 μA. This is due to the fact that the smaller sized sensors reached higher Q values which compensates for their smaller Lorentz forces.

The detf type magnetometers were less sensitive with a flux density resolution of about 70 nT/$\sqrt{}$Hz at the minimum pressure. This is due to the smaller number of turns in the excitation coil, reducing the Lorentz force. A comparison of Figs. 10 and 11 shows that both magnetometer types have a resolution of about 60 nT or 0.5° (at $B = 10$ μT) at $p = 0.2$ mbar. These values, although exceeding our initial goal, are still sufficient for navigation.

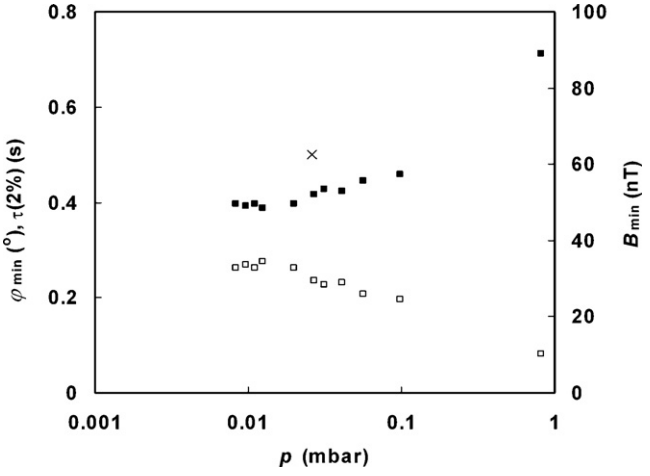

Fig. 11. Angular resolution φ_{min} and minimum detectable magnetic flux density B_{min} of a detf sensor, calculated from the measured Q-values, are marked by the filled squares. Measured flux density resolution of the torsional sensor is shown by the cross and the calculated settling time τ (2%) by the open squares.

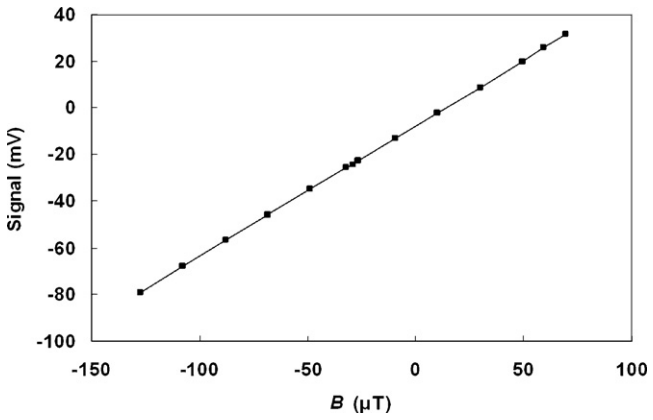

Fig. 12. Signal linearity of a torsional sensor at geomagnetic field strength.

6.2. Linearity

At geomagnetic field strength the signal was highly linear, on the order of 1%, apart from the offset due to electrostatic excitation (Fig. 12). In larger fields, however, the shape of the resonance peak becomes distorted and the signal falls below the linear response (Fig. 13). This can be understood as the onset of capacitive nonlinearity [7]. The critical vibration amplitude x_{c3e} above which the resonance peak becomes hysteretic, is given by:

$$x_{c3e} = \sqrt{\frac{32}{27\sqrt{3}}}\sqrt{\frac{k}{k_{3e}Q}} \tag{16}$$

where k is the spring constant and the third-order nonlinear spring constant is:

$$k_{3e} = 4\frac{C_0 V^2}{d^4}. \tag{17}$$

Here C_0 is resonator capacitance at rest, V the voltage across the capacitor plates, and d is the air gap between the electrode plates. Here the voltage V equals the bias voltage V_b. In a torsional resonator the spring constant and deflection can be approximated as $k \approx \kappa/c^2$ and $x \approx c\varphi$ where κ is the torsion spring constant, c the distance of the electrode centre point from the rotation axis

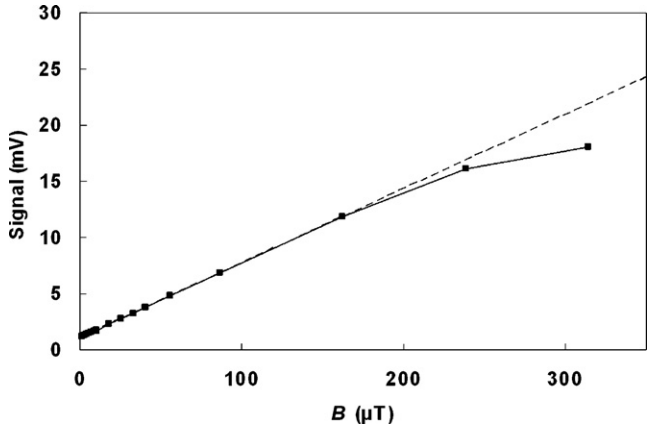

Fig. 13. Capacitive nonlinearity of a torsional magnetometer in high magnetic fields. The dashed line is a linear fit to data at $B < 100$ μT.

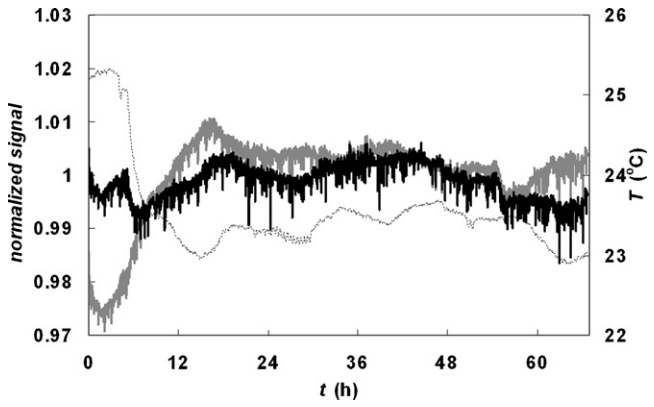

Fig. 14. Long-term stability of a 1 mm × 1 mm sized torsional sensor. Normalized signal voltage before and after temperature compensation is shown by the grey and black curves, respectively. Temperature is shown by the thin dotted curve.

and φ is the rotation angle. The calculated vibration amplitude equals x_{c3e} at a field strength $B = 150\,\mu\text{T}$ for the sensor which was used to collect the data in Fig. 13, showing good agreement between calculated and measured onset of nonlinearity.

Imperfect grounding of the moving silicon sensor structure manifests itself as the offset of the signal at zero field in Fig. 13. The ac potential of the voltage-to-current converter couples to the silicon layer through the coil-silicon capacitance. The resulting electrostatic excitation can be minimized with the adjustments of the current source (Fig. 4) but it can, on the other hand, be utilized to ensure that the VCO frequency tracks the mechanical resonance frequency at zero magnetic field where the signal otherwise vanishes.

6.3. Stability

Some preliminary long-term stability measurements were performed in a laboratory environment without active temperature regulation. The stability of a torsional sensor is shown in Fig. 14 and of a detf sensor in Fig. 15. The measurement was carried out in the ambient magnetic field. Both sensors had almost equal stability with the standard deviation of the signal less than 1% over a period of a few days. The temperature coefficient of the signal voltage was quite high, about 1%/°C, but linear temperature compensation removed most of the temperature dependency.

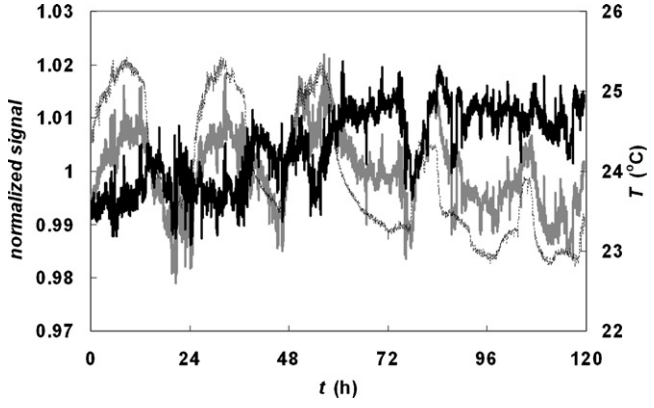

Fig. 15. Long-term stability of a detf sensor. Normalized signal voltage before and after linear temperature compensation is shown by the grey and black curves, respectively. Temperature is shown by the thin dotted curve.

7. Conclusion and outlook

We have demonstrated that navigation-grade resolution can be achieved with a 3D micromachined magnetometer at 100 μA sensor coil current per coordinate axis. Preliminary measurements showed that signal linearity and stability is sufficient for navigation as well but the temperature coefficient is quite large. As a downside, the large area of the excitation coil makes the design sensitive to electrostatic excitation. The manufacturing process allows us to integrate inertial sensors for tilt compensation on the same chip as well. The fabrication process is presently quite complicated so some simplifications are necessary to improve the yield and reduce production costs.

Packaging may become the most crucial factor determining the success of a micromechanical magnetometer owing to the high vacuum needed for good resolution. The vacuum requirement is, however, not too different from that of silicon gyroscopes and resonators. In addition, the package has to be nonmagnetic. Future work will thus concentrate on vacuum encapsulation with an anodically bonded capping wafer and getter material.

Acknowledgements

We kindly acknowledge the National Technology Agency of Finland for funding this study and R. Lindman for processing the magnetometers.

References

[1] H.H. Yang, N.V. Myung, J. Yee, D.-Y. Park, B.-Y. Yoo, M. Schwartz, K. Nobe, J.W. Judy, Ferromagnetic micromechanical magnetometer, Sens. Actuators A 97–98 (2002) 88.
[2] Zs. Kádár, A. Bossche, P.M. Sarro, J.R. Mollinger, Magnetic-field measurements using an integrated resonant magnetic-field sensor, Sens. Actuators A 70 (1998) 225.
[3] H. Emmerich, M. Schöfthaler, Magnetic field measurements with a novel surface micromachined magnetic-field sensor, IEEE Trans. Electron Dev. 47 (2000) 972.
[4] D.K. Wickenden, J.L. Champion, R. Osiander, R.B. Givens, J.L. Lamb, J.A. Miragliotta, D.A. Oursler, T.J. Kistenmacher, Micromachined polysilicon resonating xylophone bar magnetometer, Acta Astron. 52 (2003) 421.
[5] J. Kyynäräinen, J. Saarilahti, H. Kattelus, T. Meinander, M. Suhonen, A. Oja, H. Seppä, P. Pekko, H. Kuisma, S. Ruotsalainen, M. Tilli, 3D Micromechanical Compass, Proceedings of the 6th European Conference on Magnetic Sensors and Actuators, Bilbao, Spain, July 3–5, 2006, Sensor Letters, in press.
[6] K. Funk, W. Frey, Magnetic field sensor having deformable conductor loop segment, US Patent 6486665 B1 (2002).
[7] T. Mattila, J. Kiihamäki, T. Lamminmäki, O. Jaakkola, P. Rantakari, A. Oja, H. Seppä, H. Kattelus, I. Tittonen, A 12 MHz micromechanical bulk acoustic mode oscillator, Sens. Actuators A 101 (2002) 19.

Biographies

Jukka Kyynäräinen received the MSc (Tech) and the DSc (Tech) degrees from the Helsinki University of Technology, Espoo, Finland, in 1985 and 1990, respectively. From 1985 to 1997 he investigated superfluid ^{3}He at the Helsinki University of Technology and polarized targets at CERN, Geneva, Switzerland. He joined the VTT MEMS sensors group in 1999 as a senior research scientist. His current research topics include micromechanical magnetic and inertial sensors.

Jaakko Saarilahti received his DSc (Tech) degree in applied physics from the Helsinki University of Technology, Espoo, Finland in 1995. He joined VTT in 1984 and presently works as a senior research scientist dealing with fabrication technology for microelectromechanical sensors.

Hannu Kattelus received his MSc (Tech) and DSc (Tech) degrees from the Department of Electrical Engineering from the Helsinki University of Technology in 1980 and 1988, respectively. Since 1979 he has been working at VTT developing thin film processes and devices for various applications. He has authored or co-authored about 100 scientific or technical papers. Currently he heads the MEMS Technology group and is a research professor in microsystems technology.

Anu Kärkkäinen received the MSc and LicSc degrees from Helsinki University in 1985 and 1987, respectively, and the PhD degree from the Helsinki University of Technology in 2006. She worked as senior scientist at Vaisala developing different capacitive sensors and measurement systems (1986–1995). She worked as product manager at Vaisala optical sensors (1995–1998) and then she coordinated the Finnish node in the EU funded HPCN-TTN network at CSC, Finnish Supercomputing Centre (1998–2001). In 2001–2004 she worked with the VTT MEMS sensors group as project coordinator and researcher in the EU funded project EMMA, which developed capacitive MEMS components for precision applications. Since 2007 she heads the VTT MEMS Sensors group.

Tor Meinander received the LicSc (Tech) degree in 1972 from the Helsinki University of Technology. He joined VTT in 1984 and worked mainly on magnetics. He retired in 2006.

Aarne Oja received his DSc (Tech) degree in 1988 from the Low Temperature Laboratory of the Helsinki University of Technology. He moved to VTT in 1995 and is now the research director in the field of Sensor Technology. His current research interests include micromachined RF resonators, pressure and ultrasound sensors, RFID technology, and microsystems for ambient intelligence.

Panu Pekko received his MSc (physics) degree in 1997 and PhD (physics) degree in 2000 from the University of Helsinki. He made his thesis works on experimental properties of tetrahedral amorphous carbon coatings. He moved to VTT MEMS group in 2001 and is currently working as a senior research scientist. His research interests include MEMS fabrication technologies and sensor applications.

Heikki Seppä received the MSc (Tech), the LicSc (Tech), and the DSc (Tech) degrees from the Helsinki University of Technology in 1977, 1979, and 1989, respectively. From 1976 to 1979, he was an assistant at the Helsinki University of Technology, working in the area of electrical metrology. He joined VTT in 1979 and since 1989 he acts there as a Research Professor. In 1996, he acted a short period as the Research Director of VTT Automation. He has done research work on electrical metrology, in general, and on superconducting devices for measurement applications, in particular. Currently, he is doing research on DC SQUIDs, quantized Hall effect, SET-devices and microelectromechanical devices.

Mika Suhonen joined VTT in 1996. He has since worked on applying MEMS to electrical metrology and also on various MEMS sensors and fine-pointing actuators. His current research focus is on digital signal processing and simulation of MEMS.

Heikki Kuisma graduated from the Helsinki University of Technology with an MSc degree in Semiconductor Technology and Measurement Science in 1978. First he was employed as a researcher at VTT. In 1980 he joined Vaisala to work on MEMS sensors. This technology was transferred to a spin-off company, VTI Technologies, in 1991 where he has been responsible for the development of MEMS sensors. In 2005 he was nominated as a Research Director of VTI. He has obtained several patents in the field of MEMS. He has also been involved in planning and controlling both national and European MEMS and microelectronics research programs.

Sami Ruotsalainen received the MSc (Tech) degree from the Helsinki University of Technology, Espoo, Finland, in 1998. He has held various R&D positions with VTI Hamlin in Finland, Helsinki Institute of Physics at CERN, Geneva, Delphi Automotive Systems in Luxemburg and Suunto in Finland. Currently Mr. Ruotsalainen works as a Senior Lecturer, Automotive Electronics Engineering at Helsinki Polytechnic Stadia with focus on automotive systems, vehicle dynamics management and electric powertrains.

Markku Tilli obtained a degree in Materials Science (Physical Metallurgy) at Helsinki University of Technology (HUT) in 1974. Until 1980 he had various research and teaching positions at HUT specializing in crystal growth technologies. From 1981 to 1984 he managed process research and development in Silicon project at HUT silicon wafer manufacturing pilot plant. Since 1985 he has had various managing positions at Okmetic in research, development and customer support areas, now he holds a position of Senior Vice President, Research. His MEMS related activities started in 1982 when he developed a process to make double side polished silicon wafers for bulk micromachined sensors. Since then he has developed advanced new silicon wafer types for MEMS, including special epitaxial wafers, SOI and SOI wafers with buried cavities. His publication topics include oxygen precipitation in silicon, silicon crystal growth, wafer cleaning as well as silicon wafer manufacturing technologies and applications in MEMS.